Nonimmune cell–derived ICOS ligand functions as a renoprotective αvβ3 integrin–selective antagonist

Kwi Hye Koh,[1] Yanxia Cao,[1] Steve Mangos,[1] Nicholas J. Tardi,[1] Ranadheer R. Dande,[1] Ha Won Lee,[1] Beata Samelko,[1] Mehmet M. Altintas,[1] Vincent P. Schmitz,[1] Hyun Lee,[2] Kamalika Mukherjee,[3] Vasil Peev,[1] David J. Cimbaluk,[4] Jochen Reiser,[1] and Eunsil Hahm[1]

[1]Department of Internal Medicine, Rush University Medical Center, Chicago, Illinois, USA. [2]Center for Biomolecular Science and Department of Medicinal Chemistry and Pharmacognosy, University of Illinois at Chicago, Chicago, Illinois, USA. [3]Department of Medicine, Harvard Medical School and Division of Nephrology, Massachusetts General Hospital, Charlestown, Massachusetts, USA. [4]Department of Pathology, Rush University Medical Center, Chicago, Illinois, USA.

Soluble urokinase receptor (suPAR) is a circulatory molecule that activates αvβ3 integrin on podocytes, causes foot process effacement, and contributes to proteinuric kidney disease. While active integrin can be targeted by antibodies and small molecules, endogenous inhibitors haven't been discovered yet. Here we report what we believe is a novel renoprotective role for the inducible costimulator ligand (ICOSL) in early kidney disease through its selective binding to podocyte αvβ3 integrin. Contrary to ICOSL's immune-regulatory role, ICOSL in nonhematopoietic cells limited the activation of αvβ3 integrin. Specifically, ICOSL contains the arginine-glycine-aspartate (RGD) motif, which allowed for a high-affinity and selective binding to αvβ3 and modulation of podocyte adhesion. This binding was largely inhibited either by a synthetic RGD peptide or by a disrupted RGD sequence in ICOSL. ICOSL binding favored the active αvβ3 rather than the inactive form and showed little affinity for other integrins. Consistent with the rapid induction of podocyte ICOSL by inflammatory stimuli, glomerular ICOSL expression was increased in biopsies of early-stage human proteinuric kidney diseases. *Icosl* deficiency in mice resulted in an increased susceptibility to proteinuria that was rescued by recombinant ICOSL. Our work identified a potentially novel role for ICOSL, which serves as an endogenous αvβ3-selective antagonist to maintain glomerular filtration.

Introduction

Integrins are heterodimeric transmembrane glycoproteins that facilitate cellular attachment to the extracellular matrix or to ligands on other cells, and mediate multiple cellular processes such as proliferation, differentiation, adhesion, and migration (1). In the kidney, integrins are known to play critical roles in organ development, homeostasis, and renal disease progression (2, 3). Early glomerular injury involves a morphological change to podocytes, the terminally differentiated glomerular cells that are essential for kidney filtration, called foot process effacement (fusion), and often leads to proteinuria, a hallmark of many kidney diseases (4, 5). Activation of αvβ3 integrin on podocytes has been implicated in the pathogenesis of proteinuric kidney diseases such as focal and segmental glomerulosclerosis (FSGS), diabetic nephropathy (DN), and potentially several other renal diseases (6–11). In line with these findings, blocking of αvβ3 activation via antagonist treatment has been shown to significantly reduce proteinuria, kidney fibrosis, and subsequent disease progression in animal models (6, 7, 12–14).

Inducible costimulator ligand (ICOSL) (also known as B7h, GL50, B7RP-1, and B7-H2) belongs to the B7 superfamily of proteins that bind to the CD28 family of receptors on lymphocytes (15–19). ICOSL is expressed primarily by professional antigen presenting cells (APCs) such as B cells, dendritic cells, and macrophages. Similar to other members of the CD28/B7 superfamily, binding of ICOSL on APCs to ICOS on T cells leads to costimulatory signaling, resulting in multiple T cell functions (15, 17, 20). A previous publication exploring a potential functional role for the ICOS/ICOSL pathway in the kidney reported that ICOSL is induced in nephritic glomeruli (21). This leads to a local reduction of T cell and macrophage accumulation and attenuated renal injury, suggesting a protective role (21). Similarly, *Icosl* mRNA expression has been detected in some murine nonlymphoid tissues, such as kidney and testis, following lipopolysaccharide (LPS) injection (15). However, given that ICOS and ICOSL have been considered an exclusively single receptor–ligand pair (17, 22), little is known about ICOS-independent cellular functions between ICOSL and any yet-to-be identified corresponding receptors. In this study, we showed that ICOSL could directly bind and counter the negative effects of activated αvβ3 integrin on podocytes. An in silico sequence analysis of human and mouse ICOSL proteins, followed by 3-dimensional (3D) homology protein modeling, revealed that both human and mouse ICOSL contain an Arg-Gly-Asp (RGD) motif at an exposed loop region. Using surface plasmon resonance (SPR) combined with competition assays, we showed that ICOSL,
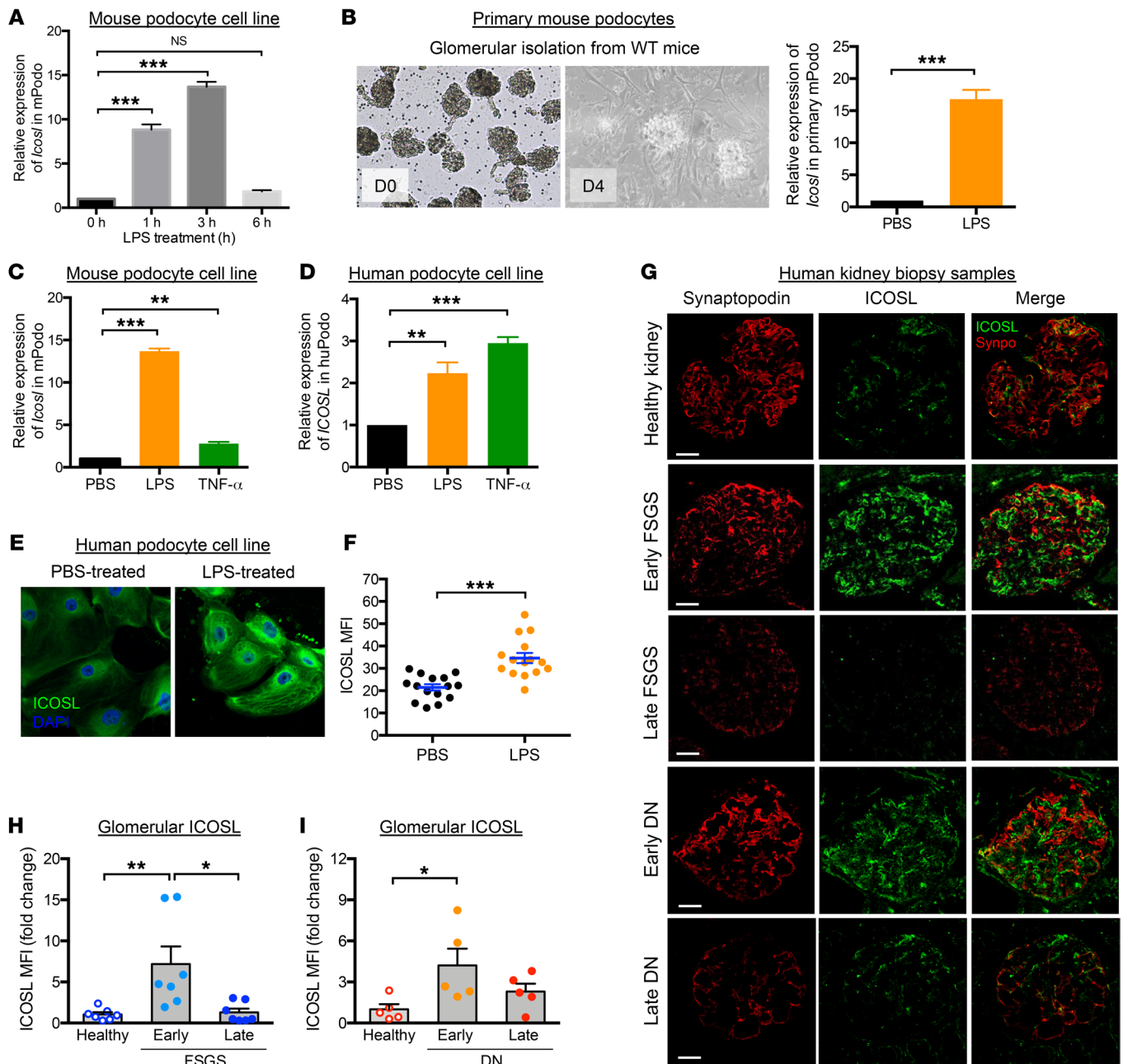
Figure 1. Increased *ICOSL* expression is an early cellular response to renal injury. Relative mRNA expression values measured by quantitative PCR targeting *ICOSL* in both mouse (**A**–**C**; mPodo) and human (**D**; hPodo) podocyte cell lines. (**A**) qPCR analysis of *Icosl* mRNA in mouse podocyte cell lines 1, 3, or 6 hours after 50 μg/ml LPS treatment, normalized with the expression level of *Gapdh* and presented relative to the expression of *Icosl* in untreated control cells. (**B**) Primary podocyte isolation from BALB/c mice by Dynabead perfusion followed by 50 μg/ml LPS treatment for 3 hours. The cells were cultured and harvested, and relative expression levels of *Icosl* were measured by qPCR. (**C**) Relative mRNA expression levels of *Icosl* in mouse podocyte cell lines treated with 50 μg/ml LPS or 100 ng/ml TNF-α for 3 hours. (**D**) Relative expression levels of *ICOSL* in human podocyte cell lines following the same treatments as in **C**. Representative images (**E**) and quantification (**F**) of immunofluorescence staining of ICOSL protein in human podocytes treated with 50 μg/ml LPS (orange dots in **F**) or PBS (black dots in **F**) as control. For quantification, cells were individually defined by tracing cell borders, and the levels of ICOSL protein expression were measured by mean fluorescence intensity (MFI) using ImageJ software (*n* = 15 cells/group). (**G**–**I**) Human kidney biopsy samples were double-stained to detect ICOSL (green) and synaptopodin (Synpo; red) by immunofluorescence staining. As depicted, analysis groups include healthy control and kidney tissues from patients with FSGS or DN at early/late stages (*n* = 5/group). The confocal micrographs were analyzed for glomerular expression of ICOSL by manually selecting glomeruli, defined by synaptopodin, as the region of interest. Representative confocal microscopic images are shown in **G**. Scale bars, 50 μm. ICOSL MFI in FSGS (**H**) or DN (**I**) groups was normalized to that of healthy controls, and data are presented as fold changes. Data are shown as mean ± SEM; *$P < 0.05$, **$P < 0.01$, ***$P < 0.001$; 1-way ANOVA with Dunnett's multiple comparison test (**A**, **C**, and **D**) or with Tukey's multiple comparison test (**H** and **I**) and Student's 2-tailed, unpaired *t* test (**B** and **F**).

through its RGD motif, directly bound αvβ3 integrin. $Icosl^{-/-}$ (Icosl-KO) mice were significantly more susceptible than control mice to LPS-induced proteinuria and STZ-induced DN phenotypes. Bone marrow (BM) transplant experiments revealed that ICOSL's protective abilities arise from its nonhematopoietic expression. Finally, administration of ICOSL protein to Icosl-KO mice reduced their susceptibility to LPS-induced proteinuria. Taken together, our work reveals what we believe is a novel role for ICOSL in countering activated αvβ3 integrin. These findings advance our understanding of diseases that stem from aberrant integrin signaling and offer the potential to explore the use of endogenous integrin antagonists as novel therapies.

Results

Increased ICOSL expression is an early cellular response to renal injury. Earlier work by Swallow et al. suggested that *Icosl* mRNA expression was not limited to hematopoietic cells and showed that expression was high in mouse kidney and testes after stimulation by LPS injection (15). We confirmed and extended these observations using cultured renal cells (podocytes and proximal tubules). Inflammatory signals such as LPS and tumor necrosis factor alpha (TNF-α) induced changes in ICOSL expression in renal cells. *Icosl* mRNA expression was significantly increased in both renal cell types, reaching a peak 3 hours after LPS treatment, followed by a dramatic decrease 6 hours after injection (Figure 1A and Supplemental Figure 1A; supplemental material available online with this article; https://doi.org/10.1172/JCI123386DS1). In particular, mouse podocytes (both primary and conditionally immortalized cells) significantly increased *Icosl* expression in response to LPS stimulation (Figure 1, A and B). Similar results were observed in human podocytes or when cells were treated with TNF-α (Figure 1, C and D). Antibody staining showed that LPS-treated human podocytes displayed significantly elevated levels of ICOSL protein (Figure 1, E and F). Consistently, renal biopsies from patients with FSGS and DN, diseases where the primary lesion involves morphological damage to podocytes in the form of foot process effacement leading to proteinuria, displayed robust glomerular ICOSL expression at early stages of the disease followed by a drastic decline at later stages. This decline mirrored the loss of the podocyte marker protein synaptopodin (ref. 23 and Figure 1, G–I). These findings imply that increased ICOSL is an early cellular response to renal injury.

ICOSL protein is a ligand for αvβ3 integrin. An in silico analysis showed that ICOSL contains an RGD sequence, a known integrin-binding motif, unlike other B7 family members (such as B7.1, B7.2, and PDL-1) (Supplemental Figure 2A). Multiple alignments of ICOSL protein sequences indicate that the RGD motifs were highly conserved across different species (Supplemental Figure 2B). ICOSL is a transmembrane protein composed of a membrane-distal IgV domain, a membrane-proximal IgC domain, and a cytoplasmic domain (Supplemental Figure 3A). In evolutionarily advanced vertebrates such as human, chimpanzee, monkey, and wolf, the RGD sequences are located in the IgV domain. In contrast, mouse ICOSL has its RGD domain in the IgC domain (Supplemental Figure 2B). 3D homology modeling revealed that both human and mouse ICOSL contain an RGD motif at an exposed loop region (Supplemental Figure 3B), indicating that this RGD motif is

accessible to integrin and potentially functional. We performed SPR analysis (Figure 2A) to determine the binding affinity between recombinant ICOSL protein (Supplemental Figure 3, C and D) and αvβ3 or α3β1 integrin, the 2 major integrins expressed on podocytes (2). We first sought to determine if the ICOSL protein could directly bind to αvβ3, an RGD-dependent integrin, in the presence of Mn^{2+}, a potent activator of integrin (9). ICOSL, but not the RGD-lacking B7.1, exhibited high-binding affinity for active αvβ3 integrin (K_D = 16.2 ± 4.0 nM for human, K_D = 24.2 ± 6.5 nM for mouse; Figure 2, B and E and Supplemental Figure 4A). However, the binding affinity was significantly lower when αvβ3 integrin was in its inactive form (K_D = 412 ± 164 nM for human, K_D ≥ 2 mM for mouse; Figure 2, C and F). Addition of synthetic cyclic RGD (cRGDfv) outcompeted ICOSL-integrin interactions, suggesting that the binding site on ICOSL was indeed the RGD sequence (Figure 2, D and G). In contrast to αvβ3, α3β1, an RGD-independent laminin-binding integrin, showed no appreciable binding to ICOSL (K_D ≥ 2 mM; Supplemental Figure 4, B–D). As expected, the well-characterized traditional binding partner for ICOSL, ICOS, displayed a high binding affinity (K_D = 5.0 ± 1.4 nM; Supplemental Figure 4E). Next, we tested if ICOSL could bind to αvβ3 integrin in the presence of the physiologically relevant divalent ions Ca^{2+} and Mg^{2+}. Similar to when Mn^{2+} is present, ICOSL exhibited high binding affinity for αvβ3 integrin (K_D = 21.3 ± 1.2 nM; Figure 2H) at low concentrations (0.2 mM Ca^{2+} and 0.1 mM Mg^{2+}), a condition in which integrin activation is normally increased (24, 25). However, this strong binding affinity was greatly decreased (K_D = 400 ± 40 nM; Supplemental Figure 5) under normal resting serum concentrations of Ca^{2+} (2 mM) and Mg^{2+} (1 mM), consistent with our findings that ICOSL preferentially bound to the active form of αvβ3 rather than to the inactive one. To verify that ICOSL interacts with αvβ3 integrin through its RGD motif, we generated RGD-mutated mouse ICOSL protein and assessed its ability to bind mouse αvβ3 integrin (Figure 2I). Site-directed mutagenesis was used to replace the RGD motif with the amino acids AAA in mouse ICOSL. DNA sequencing was performed to confirm the change (Figure 2, H and I, top). Indeed, the binding affinity of ICOSL toward αvβ3 was markedly lower when the RGD sequences were mutated to AAA (K_D = 0.83 ± 0.80 mM; Figure 2I). These results indicate that the RGD motif in ICOSL is critically important for binding to active αvβ3 integrin. We further tested ICOSL's binding specificity toward other RGD-binding integrins, αIIbβ3 and αvβ5. Interestingly, ICOSL, despite the presence of an RGD motif on these integrins, selectively bound to αvβ3 but not to αIIbβ3 or to αvβ5 (Supplemental Figure 6). Together, these data suggest that ICOSL preferentially binds to active αvβ3 with high affinity through its RGD motif, rather than to other integrins such as α3β1, αIIbβ3, and αvβ5.

ICOSL regulates αvβ3 integrin–dependent adhesion in human podocytes. To investigate the role of ICOSL–αvβ3 integrin pairing in podocyte function, we employed an adhesion assay using cultured human podocytes (Figure 3A). In line with the selective binding of ICOSL to active αvβ3, podocyte adhesion to ICOSL-coated plates was significantly increased when αvβ3 was activated by Mn^{2+}, and it was completely inhibited by either cRGDfv or anti-β3 antibodies (Figure 3, B and C). We observed comparable results when podocytes were grown on plates coated with the RGD-containing extracellular matrix
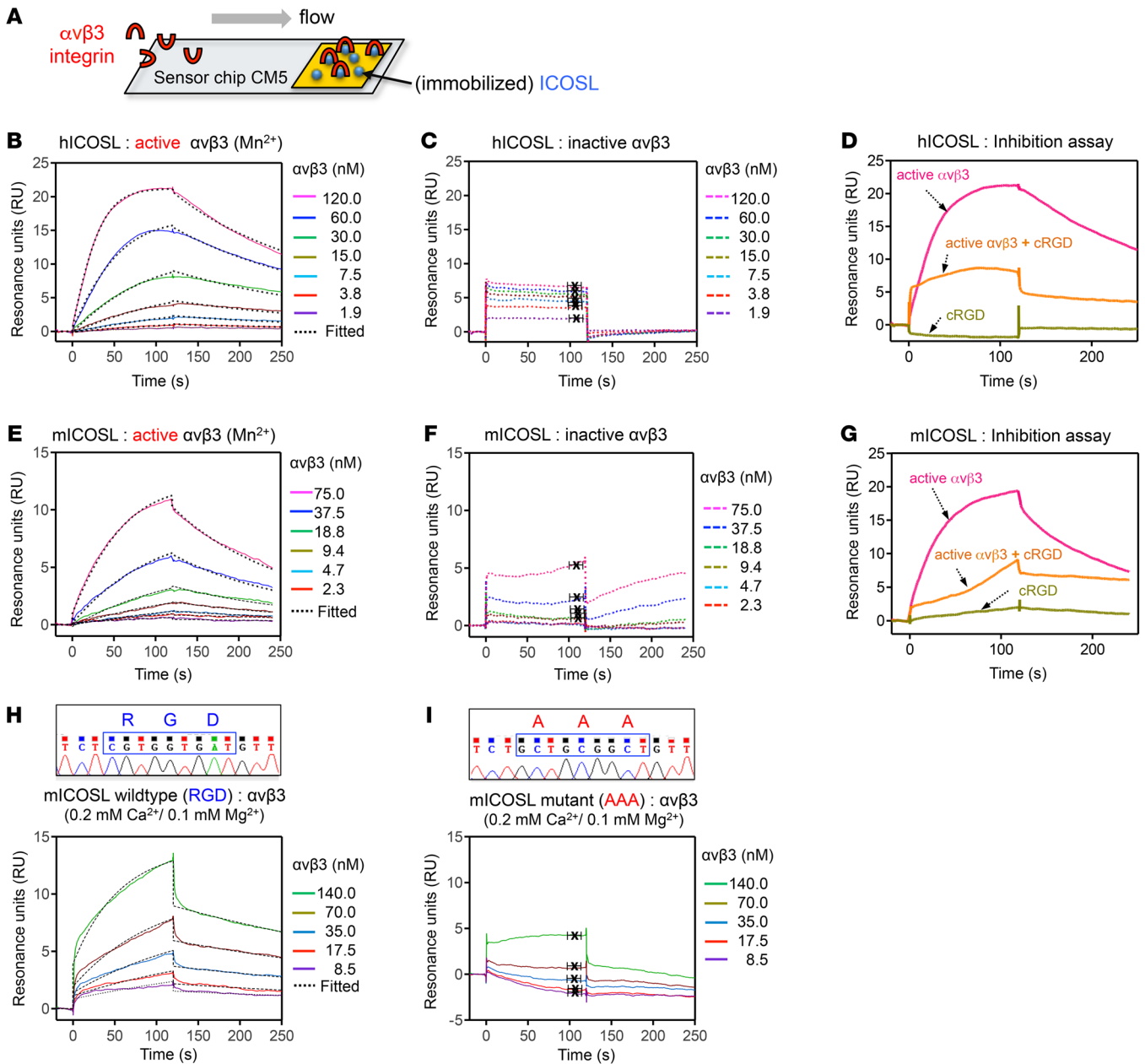
Figure 2. ICOSL binds to active αvβ3 integrin through its RGD motif. (**A**) Schematic of a gold surface with ICOSL protein on a sensor chip CM5 and associated protein (αvβ3 integrin) over which buffer is flown in SPR assay. (**B–I**) SPR sensorgrams depicting interaction of immobilized human ICOSL (hICOSL, **B–D**) or mouse ICOSL (mICOSL, **E–I**) with αvβ3 integrin. These bindings were tested in the presence (**B** and **E**, active form of αvβ3) or absence (**C** and **F**, inactive form of one with EDTA in the binding buffer) of Mn^{2+}. (**D** and **G**) SPR used in an inhibition experiment with cRGDfv. Injection of αvβ3 integrin only (**D**, 120 nM αvβ3 or **G**, 150 nM αvβ3) resulted in a binding signal for immobilized hICOSL or mICOSL alone (pink line). Preincubation with cRGDfv (3 μM or 15 μM) significantly reduced the binding for ICOSL, indicating that the RGD peptide competes with ICOSL for binding to αvβ3 (orange line). cRGDfv alone was used as a control (green line). (**H** and **I**) SPR sensorgrams showing the binding between WT (**H**) or mutant (**I**) mICOSL protein and αvβ3 integrin in the presence of physiologically relevant divalent ions, Ca^{2+} (0.2 mM) and Mg^{2+} (0.1 mM). The average K_D values were determined from at least 3 independent experiments. Rate constants (k_a and k_d) were determined by kinetic fitting (black dotted line) of the sensorgrams using 1-to-1 Langmuir binding equation, and K_D values for **B**, **E**, and **H** were calculated by k_d/k_a (**B**, K_D = 16.2 ± 4.0 nM for hICOSL/αvβ3 with Mn^{2+}; **E**, K_D = 24.2 ± 6.5 nM for mICOSL/αvβ3 with Mn^{2+}; **H**, K_D = 21.3 ± 1.2 nM for WT mICOSL/αvβ3 with Ca^{2+}/Mg^{2+}). K_D values for **C**, **F**, and **I** were calculated from steady-state affinity fittings (**C**, K_D = 411.8 ± 164.1 nM for hICOSL/αvβ3; **F**, K_D ≥ 2 mM for mICOSL/αvβ3; **I**, K_D = 0.83 ± 0.8 mM for mutant mICOSL/αvβ3 with Ca^{2+}/Mg^{2+}).

protein vitronectin (Figure 3D). Additionally, *ICOSL* knock-down (Supplemental Figure 7A) led to significantly decreased αvβ3-mediated adhesion on vitronectin-coated surfaces (Supplemental Figure 7B), but showed no difference on collagen I–coated plates (Supplemental Figure 7C). Glycosylation, a com-

mon posttranslational modification, often alters the structure and function of proteins (24). To determine if ICOSL's glycosylation state impacts its functionality, we evaluated podocyte adhesion to glycosylated or deglycosylated ICOSL. Peptide-N-glycosidase F–treated (PNGaseF-treated) ICOSL produced lower molecular
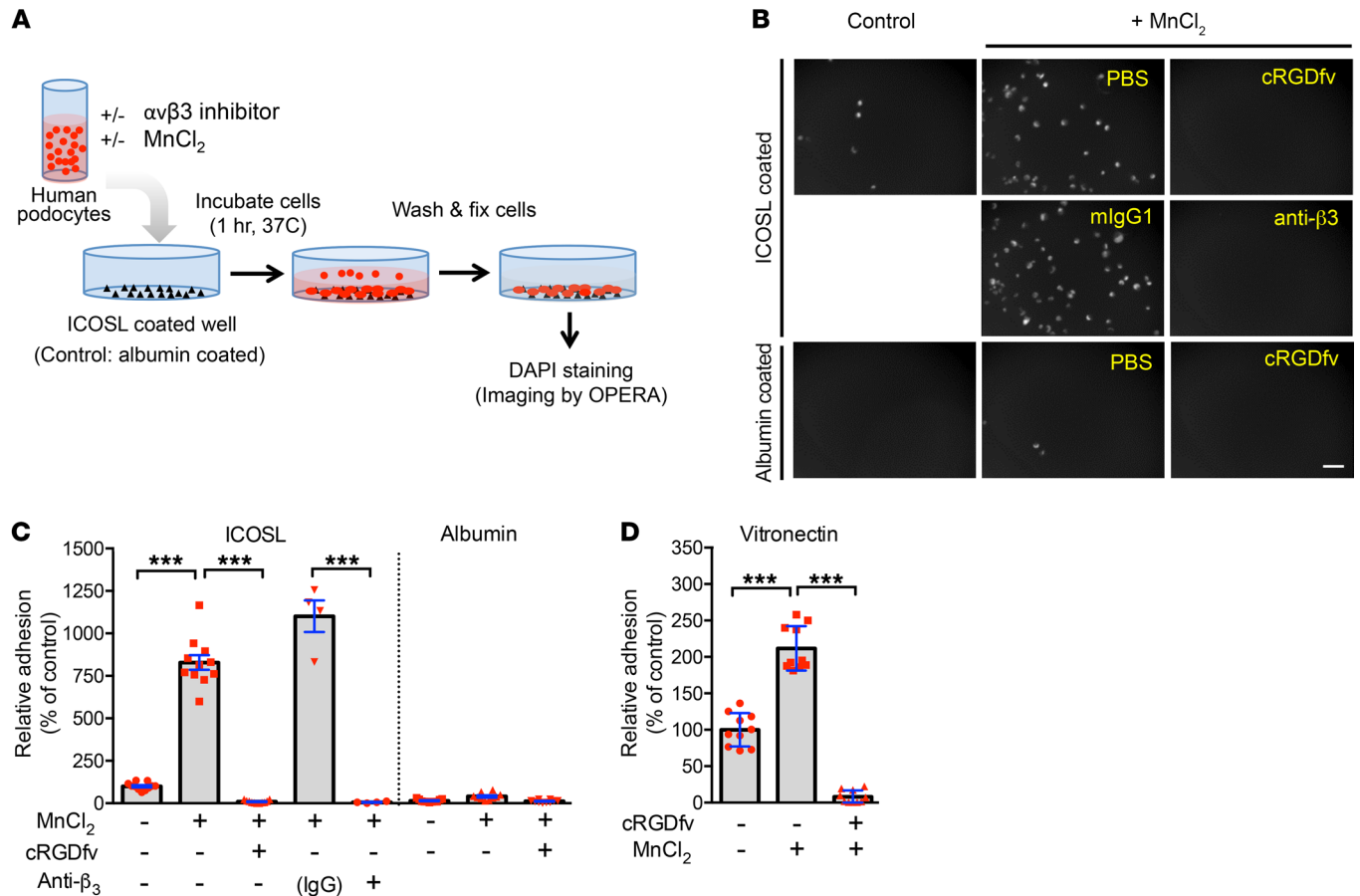
Figure 3. ICOSL regulates αvβ3 integrin–dependent adhesion in human podocytes. (**A**) Schematic representation of the protocol to measure relative cell adhesion levels in cultured human podocytes. Image analysis and quantification by high-content screening technology were described in Methods. (**B**) Phase-contrast microscopy images show that cultured human podocytes confer enhanced adhesion to ICOSL mediated by β3 integrin treated with Mn^{2+}, but do not adhere on albumin (protein control). Increased adhesion levels were completely prevented by incubation with the integrin inhibitors, including cRGD peptide and anti-β3 integrin antibody. Scale bar 100 μm. (**C**) Quantification of the cell adhesion using the images in **B**. ICOSL induced cell adhesion to RGD-dependent β3 integrin on cultured podocytes. (**D**) Cell adhesion analysis of cultured podocytes plated on vitronectin. Data are shown as mean ± SD; ***$P < 0.001$; 1-way ANOVA with Tukey's multiple comparison test (**C** and **D**).

weight bands, representing deglycosylated forms of ICOSL (Supplemental Figure 8B). Our SPR data (Figure 2E vs. Supplemental Figure 8A) closely mirrored our adhesion assay data (Supplemental Figure 8, C and D), indicating that glycosylation state does not affect ICOSL's ability to bind active αvβ3 nor does it affect the adhesive behavior of podocytes. Our data suggest that ICOSL's RGD motif is functionally active and important for αvβ3 integrin–mediated podocyte adhesion, regardless of glycosylation state.

ICOSL plays a protective role during kidney injury. To test ICOSL's contribution to kidney function, we induced kidney injury using 2 different in vivo mouse models: LPS-induced acute kidney damage and streptozotocin-induced (STZ-induced) DN. Using previously reported methods (25), *Icosl*-KO mice treated with LPS displayed high mortality rates (80%, data not shown), indicating that these mice are vulnerable to LPS-induced kidney damage. Using reduced LPS doses, albumin-to-creatinine ratio (ACR) and blood urea nitrogen (BUN) measurements taken 24 hours after injection showed that *Icosl*-KO mice exhibit a significant loss in kidney function (ACR: 1812.1 ± 207.9 μg/mg, BUN: 272.0 ± 21.8 mg/dl) when compared with WT mice (ACR: 746.3 ± 109.5 μg/mg, BUN: 89.5 ± 16.0

mg/dl) (Figure 4, A and B). Similar results were obtained using the STZ-induced model of DN (Figure 4, C–F). Interestingly, *Icosl*-KO mice showed early and severe hyperglycemia after 125 mg/kg STZ injection, a high mortality rate (50%) after 21 days, and significantly high levels of proteinuria (Supplemental Figure 9, A–C). Consistent with LPS injection, *Icosl*-KO mice were significantly vulnerable to kidney damage caused by STZ injection. To extend the time frame of our study and allow for weekly blood glucose and ACR measurements, WT and *Icosl*-KO mice were injected with a low dose of STZ (100 mg/kg) (Figure 4, C and D). The STZ-induced diabetic *Icosl*-KO mice showed a significant and persistent rapid increase in blood glucose levels when compared with WT diabetic mice (Supplemental Figure 9D). Consistent with the high blood glucose levels, the *Icosl*-KO mice displayed increased overall proteinuria levels, and BUN levels were elevated at 7 and 14 weeks compared with diabetic WT mice (Figure 4, C and D). Although there were no histological alterations with light microscopy (data not shown), the kidneys of these *Icosl*-KO mice had severe podocyte foot process effacement 14 weeks after STZ injection as shown by electronic microscopy (Figure 4, E and F). Loss of ICOSL accelerates renal function decline
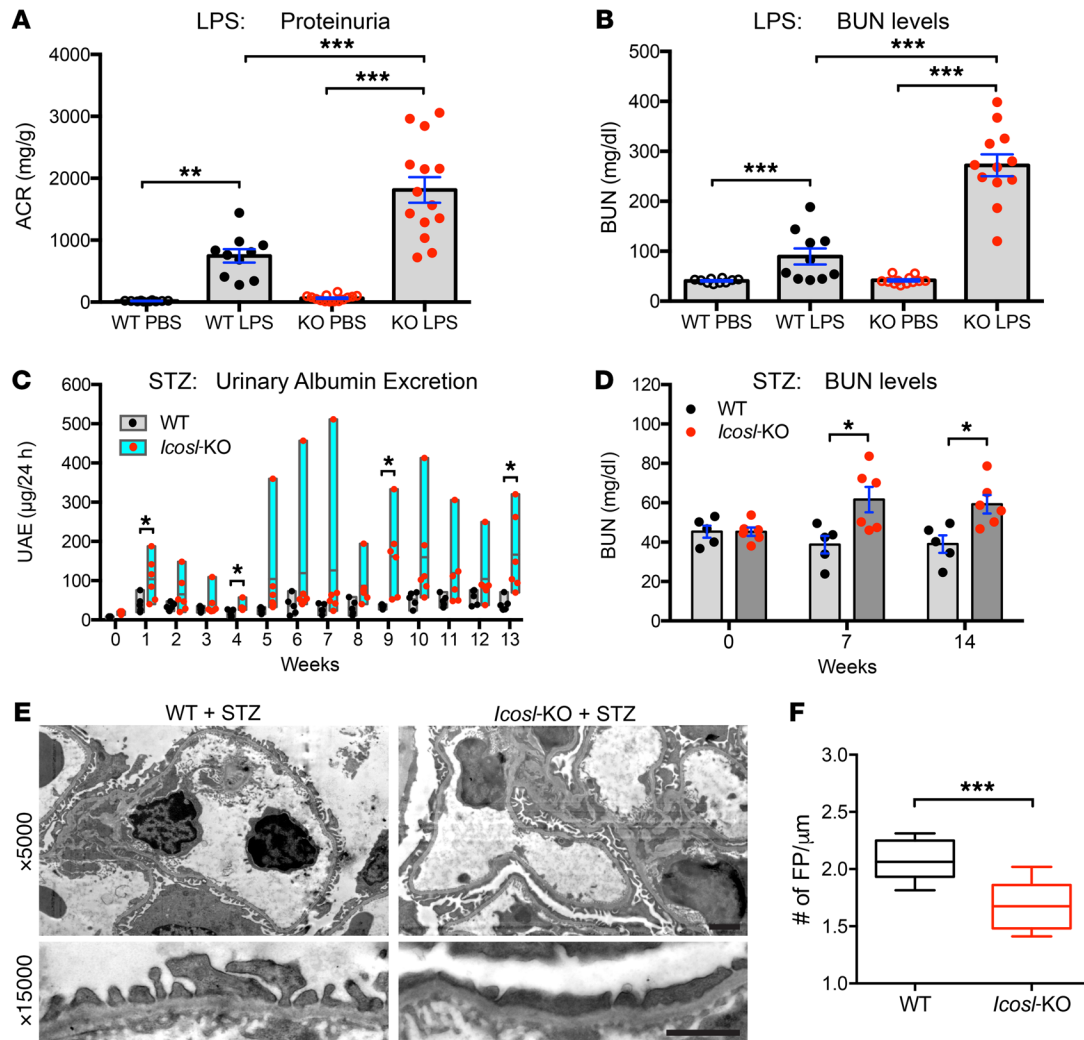
Figure 4. ICOSL plays a protective role during kidney injury. (**A** and **B**), BALB/c WT and *Icosl*-KO mice were injected with either PBS or LPS (2.5 mg/kg body weight), then urine and blood were collected 24 hours later (*n* = 10 for WT PBS, *n* = 10 for WT LPS, *n* = 14 for KO PBS, *n* = 14 for KO LPS). (**A**) Urinary albumin and creatinine were measured using a mouse albumin ELISA kit and a creatinine assay kit, respectively. ACR ratio (mg/g) was calculated and used as a parameter to determine proteinuria. (**B**) Renal function was evaluated by measuring BUN levels as described in Methods. (**C** and **D**) Both BALB/c WT (black dots) and *Icosl*-KO (red dots) mice developed hyperglycemia after STZ injection (*n* = 5–6 per group). (**C**) The floating bar graph indicates urinary albumin excretion levels. (**D**) BUN levels. (**E**) Transmission electron microscope (TEM) analysis of PFA-fixed kidney glomeruli from STZ-induced WT and *Icosl*-KO mice (14 weeks after STZ injection). Top, TEM images displaying capillary loops at ×5000 magnification. Bottom, high magnification of podocyte foot processes (×15,000) highlighting mild effacement in the WT group and more severe effacement in the *Icosl*-KO group. Scale bars, 2 μm. (**F**) Quantification of foot process (FP) effacement using the TEM images (**E**). Boxes and line represent mean ± SEM and whiskers showing minimum and maximum points (*n* = 10 biological samples per group). Data are mean ± SEM; *P < 0.05, **P < 0.01, ***P < 0.001; 1-way ANOVA with Tukey's multiple comparison test (**A** and **B**) or multiple unpaired *t* test with the Holm-Sidak comparisons test (**C** and **D**) or Student's 2-tailed, unpaired *t* test (**F**).

in the context of DN. These results raised an interesting possibility that ICOSL may play a protective role in maintaining the integrity of kidney tissue.

Nonhematopoietic ICOSL protects against LPS-induced kidney injury. We next sought to confirm the renoprotective role of nonhematopoietic ICOSL. Bone marrow (BM) chimeric mice were generated by transferring isolated BM cells from BALB/c WT and *Icosl*-KO (donor) mice into irradiated WT and/or *Icosl*-KO (recipient) mice as outlined in Figure 5A. WT mice given BM cells from WT or *Icosl*-KO mice exhibited similar ACR levels (WT to WT and KO to WT), whereas *Icosl*-KO mice given BM cells from either WT or *Icosl*-KO mice showed significantly higher levels of proteinuria,

indicating that nonhematopoietic ICOSL plays an important role in protection against LPS-induced kidney dysfunction (Figure 5B). To test whether the renoprotective role of ICOSL is independent of its traditional immune-related partner, ICOS, we evaluated the effect of T cell depletion (absence of ICOS) on LPS-induced proteinuria in both WT and *Icosl*-KO mice. As expected, T cell depletion did not change the ACR levels in either WT or *Icosl*-KO mice following LPS injection (Supplemental Figure 10), suggesting that the renoprotective effect of ICOSL is likely not ICOS-dependent.

Injection of ICOSL rescues kidney injury in Icosl-KO mice. We tested our hypothesis that ICOSL acts in a renal protective manner by examining the effects of exogenously administering ICOSL protein
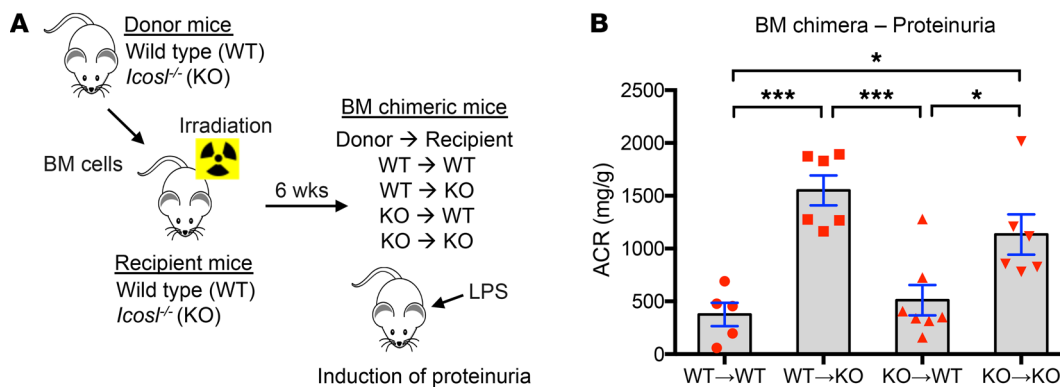
Figure 5. Loss of nonhematopoietic ICOSL aggravates LPS-induced kidney injury. (**A**) Schematic experimental design for BM chimeric mice generation. In brief, BM cells were isolated from donor mice (WT and *Icosl*-KO) and then transferred into irradiated recipient mice (WT and *Icosl*-KO) on day 0. The 4 types of BM chimera mice were produced: WT donor cells into WT recipients, WT donor cells into KO recipients, KO donor cells into WT recipients, and KO donor cells into KO recipients. Six weeks after engraftment, the BM chimeric mice were injected with LPS (2 mg/kg body weight). (**B**) Urine was harvested from each group of mice 24 hours after LPS administration (*n* = 5–7 per group from 2 independent experiments). Data are mean ± SEM; **P* < 0.05, ***P < 0.001; 1-way ANOVA with Tukey's multiple comparison test.

in *Icosl*-KO mice that had been subjected to LPS-induced kidney injury. Mice treated with ICOSL protein showed a significant reduction in ACR levels, as compared with controls injected with bovine serum albumin (BSA), both at 12 hours (single ICOSL/BSA dose of 1 mg/kg body weight) and 24 hours (2 ICOSL/BSA doses) after LPS injection (Figure 6A). The administration of recombinant ICOSL greatly restored kidney function in response to LPS in *Icosl*-KO (Figure 6B) and produced similar protective effects in WT mice (Supplemental Figure 11). A similar trend of reduced proteinuria was observed when we treated STZ-induced diabetic *Icosl*-KO mice with the administration of ICOSL twice a week for 4 weeks (*P* = 0.0535, Supplemental Figure 12). To assess the in vivo half-life of exogenously administered ICOSL, we performed plasma pharmacokinetic (PK) analysis for ICOSL after a single intravenously administered dose (1 mg/kg body weight) in *Icosl*-KO mice (Supplemental Figure 13). The PK evaluation showed that the mouse that was intravenously injected with ICOSL protein at a dose that provided therapeutic efficacy in rescue experiments (detailed above) exhibited a 2-phase clearance from plasma with a rapid initial clearance ($t_{1/2}\alpha$ = 0.06 hour) and a prolonged terminal-phase plasma half-life ($t_{1/2}\beta$ = 18.6 hours). Together, these data strongly suggest that exogenously administered ICOSL, serving as a potential therapeutic option, reverses disease progression and improves kidney function. To further test if the renoprotective effect of ICOSL is dependent on its RGD motif, *Icosl*-KO mice were treated with either WT (RGD) or mutant (AAA) ICOSL protein using a single dose 1 hour after LPS injection (Figure 6C). LPS-induced proteinuria was significantly reduced using WT ICOSL but not by mutant protein in *Icosl*-KO mice (Figure 6D), supporting our assertion that the RGD sequence on ICOSL is essential for its protective role.

Discussion

ICOSL is a member of the B7 superfamily of proteins (19, 20) whose study has been limited to outcomes related to its binding with its traditional partner, ICOS. This binding is critical for T cell activation and for the control of T cell–mediated immune responses (15–18). In the present study, we demonstrated that

ICOSL bound activated αvβ3 integrin on podocytes and modulated their adhesive characteristics. Our data suggested that this binding provided a mechanism for renoprotection by presumably modulating αvβ3 integrin–dependent signaling (Figure 7).

As previously mentioned, Odobasic et al. hinted that ICOSL may play a role in lessening the severity of kidney damage in a mouse model of crescentic glomerulonephritis (GN) (21), but this study narrowly focused on direct ICOS-ICOSL interactions within the kidney. What is becoming increasingly evident is that proteins that were once thought to be exclusively part of the immune response are also expressed on and functionally play a role in nonimmune cells. We were prompted to look more closely at ICOSL in the context of kidney disease since its expression was reported to be elevated in the kidney in response to LPS (15). Indeed, our results confirm this finding and we extend the specificity of this expression to the glomerulus in general and to podocytes in particular (Figure 1). Taking advantage of our expertise with cultured mouse and human podocyte cells as well as primary mouse podocytes, we observed a rapid rise in ICOSL expression in mere hours after an immune stimulus (Figure 1, A–F). Human biopsy samples showed similar results where glomerular ICOSL expression greatly increased at early stages of kidney disease then dropped at later stages (Figure 1, G–I). A rapid increase in ICOSL expression at the early stages of kidney injury is in accordance with a previous report that showed a related molecule in the B7 superfamily (B7.1) also increased expression in response to LPS injection (26). To date, all evidence suggests that there is a substantial increase in both *ICOSL* mRNA and protein expression levels at very early stages of renal pathogenesis. A comprehensive examination of the ICOSL protein structure revealed that unlike other members of the B7 costimulatory family of molecules, ICOSL contained an RGD motif (Figure 2). A survey of available databases showed that the RGD motif was highly conserved across several different species (Supplemental Figure 2B). This was intriguing, and pointed to the possibility that ICOSL could be functioning within the kidney/podocyte by binding not to its traditional immune-related partner (ICOS), but instead to the well-studied and podocyte-expressed αvβ3 integrin. Our group, along with others, has
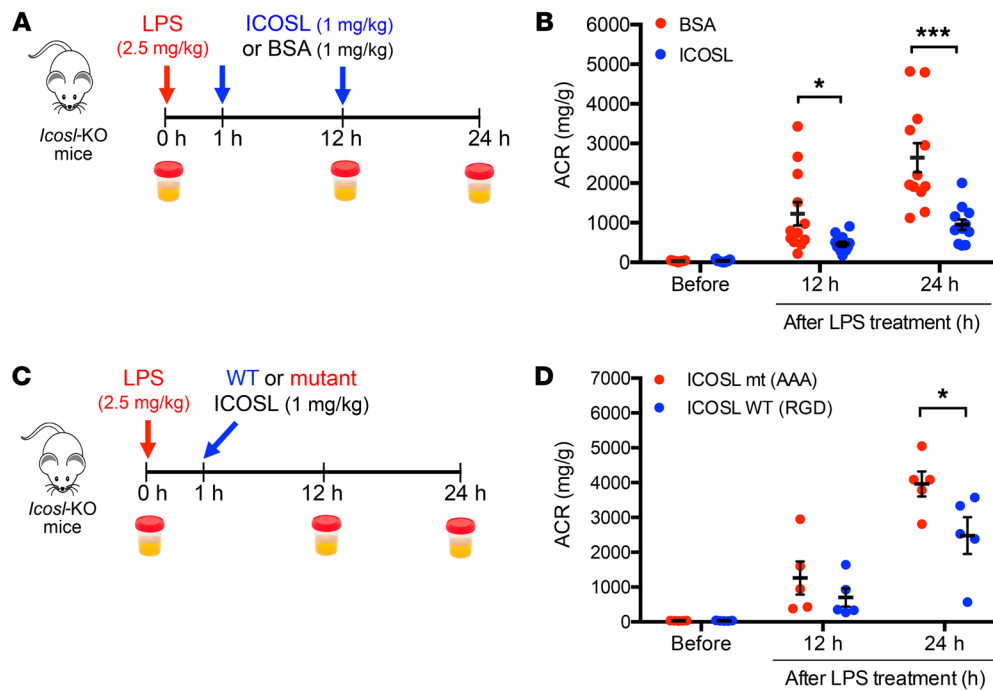
Figure 6. Administration of ICOSL reverses proteinuria in LPS-injected *Icosl*-KO mice. Schematic representation of the experimental design (**A**). In brief, *Icosl*-KO mice were challenged with 2.5 mg/kg LPS, then injected intravenously (i.v.) with mouse ICOSL protein (1 mg/kg) or BSA (1 mg/kg) as a protein control 1 and 12 hours after LPS injection. Urine samples were collected at time points, 0, 12, and 24 hours after LPS administration for ACR measurement. (**B**) ACR levels in *Icosl*-KO mice treated with either ICOSL protein (blue dots) or BSA (red dots) (*n* = 12 per group from 2 independent experiments). Schematic representation of the experimental design (**C**). *Icosl*-KO mice were challenged with 2.5 mg/kg LPS, then injected i.v. with either WT (RGD) or mutant (AAA) mouse ICOSL protein (1 mg/kg) 1 hour after LPS injection. (**D**) ACR levels in *Icosl*-KO mice treated with either WT (blue dots) or mutant (red dots) ICOSL (*n* = 5 per group from 1 experiment). Data are mean ± SEM; *$P < 0.05$, ***$P < 0.001$; multiple unpaired *t* test with the Holm-Sidak comparisons test (**B** and **D**).

highlighted the importance of signaling through this integrin (6-9, 12). We subsequently demonstrated direct binding between ICOSL and αvβ3 integrin using the highly sensitive technique of SPR (Figure 2, C–I). Site-directed mutagenesis combined with SPR analyses revealed that the RGD motif in ICOSL was critically important for binding to αvβ3 integrin (Figure 2, H and I). Furthermore, our analysis revealed that this binding is (a) highly selective for αvβ3 but not for other integrins such as α3β1, αIIbβ3, and αvβ5 (Figure 2 and Supplemental Figures 4–6); (b) dependent on the activation state of αvβ3 integrin (Figure 2 and Supplemental Figure 5); and (c) relatively strong with a high binding affinity (average K_D = 10–30 nM). At the cellular level, we confirmed that adhesion of human podocytes to ICOSL protein was dependent on the activation status of αvβ3 integrin (Figure 3). This set of results points to a mechanism whereby podocytes can mount a fine-tuned response to counterbalance a harmful over-activation of αvβ3 integrin during injury (Figure 7). This is physiologically relevant because extra-renal immune cells secrete permeability factors such as suPAR, which activate αvβ3 integrin on podocytes, leading to podocyte foot process effacement and the development of proteinuria (25, 27).

The importance of ICOSL's role in protecting the kidney filter was made strikingly clear when we challenged *Icosl*-KO mice with an inflammatory LPS stimulus, or induced a state of diabetic nephropathy via STZ injection (Figure 4). In both instances, conventional doses resulted in severe reactions in the KO mice. These experiments revealed the importance of having ICOSL expression, but did not definitively address the question of its source

since our KO was global in nature. Being aware of ICOSL's significant and well-documented role as a costimulatory ligand for ICOS in immune-related responses, we set out to determine if the hematopoietic system was involved in the apparent protective affects we observed. Our bone marrow chimera study set out to address this question and showed that induced ICOSL generated from nonlymphoid cells is important in the reduction of proteinuria after LPS-induced kidney injury (Figure 5). Since it is known that ICOS is exclusively expressed in T cells and its expression is induced upon cell activation, we tested if T cell depletion (resulting in an absence of ICOS) could impact the renoprotective effect of ICOSL. T cell depletion did not change the ACR levels of LPS-injected mice (Supplemental Figure 10). The results of our rescue experiments (Figure 6 and Supplemental Figures 11 and 12) strongly suggest that ICOSL has the potential to act as a powerful therapeutic option for some forms of kidney disease.

Understanding the mechanisms leading to glomerular injury and the endogenous agents that protect against it could foster the development of precise therapies that stop or delay disease progression. αvβ3 integrin activation is known to be involved in the initiation of glomerular damage (6–11, 28) and is possibly induced by physiological activators such as suPAR and TNF-α. Blocking or abrogating αvβ3 activation via antagonist treatment has been shown to significantly reduce proteinuria, kidney fibrosis, and subsequent disease progression in animal models (6, 7, 12–14). Our studies show that ICOSL is an endogenous protective agent that can counteract αvβ3 integrin activation. The initially elevated ICOSL expression
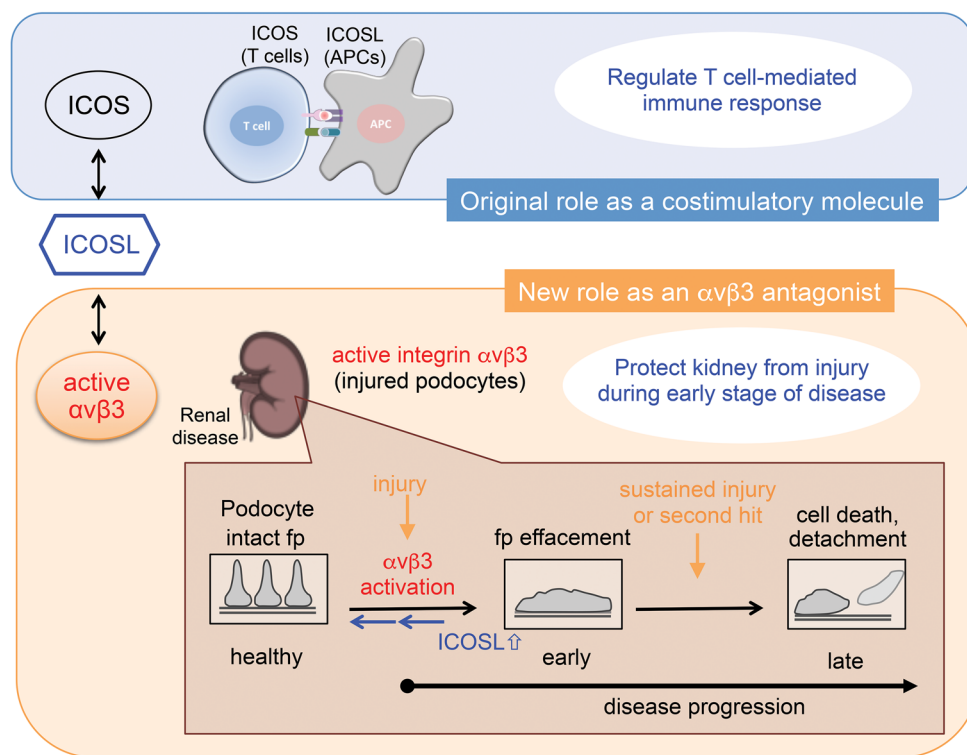
Figure 7. Schematic model of ICOSL's functions. In this study, it is shown that ICOSL binds podocyte αvβ3 integrin through its RGD motif. Kidney injury results in a rapid increase of ICOSL expression, leading to podocyte protection by blocking active αvβ3 integrin. ICOSL acts as a regulatory brake to modulate active αvβ3 integrin–mediated signaling. Fp, foot process.

levels diminished in concert with disease progression, and restoration of ICOSL by exogenous application improved renal function in mice (Figure 6 and Supplemental Figures 11 and 12). This is clear evidence that an ICOSL-based therapy is a promising therapeutic strategy to reverse disease progression. However, given that ICOSL is one of many endogenous proteins that are highly prone to enzymatic degradation, improvement of its pharmacokinetic properties is required to enhance efficacy in vivo. Moreover, identification of intrinsic factors and conditions triggering renal ICOSL induction will help effectively and safely target the disease.

Our work leaves some questions. What regulates the interplay between ICOSL and αvβ3 integrin on the surface of podocytes? How does this interplay regulate the effacement process and the cell's adhesive properties? These questions deserve further investigation. Our study did not precisely determine the subcellular level at which ICOSL and αvβ3 integrin interact. For example, our study does not clarify if ICOSL binds αvβ3 integrin in a *cis* (both proteins expressed on the same podocyte cell membrane) or *trans* (each protein expressed on separate, interdigitating podocyte cell surfaces) fashion. It cannot be ignored that αvβ3 integrin is reported to be widely expressed in various cell types other than podocytes, such as endothelial cells, fibroblasts, epithelial cells, osteoblasts, and smooth muscle cells (29). These observations were undoubtedly the impetus to test the efficacy of αvβ3 integrin–blocking drugs on a variety of disease conditions. Our current study provides what we believe is a novel mechanism that could be exploited to provide new therapeutic targets, the binding of ICOSL to αvβ3 integrin, and the resulting modulation of aber-

rant integrin signaling (Figure 7 and refs. 14, 30). Given the wide variety of tissues expressing αvβ3 integrin outlined above, it is tempting to speculate that the findings contained in this study are not limited to podocytes and may have far-reaching implications for a variety of disease conditions.

Our study uncovers that ICOSL, beyond its traditional costimulatory function, protects the kidney filter from injury by serving as a potent endogenous αvβ3-selective antagonist. This newly discovered protective role for ICOSL has allowed us to better understand the pathogenesis of αvβ3 integrin–mediated podocyte damage and offers promising novel avenues to pursue therapeutics for renal disease as well as disease conditions arising from aberrant αvβ3 integrin activation.

Methods

Mice. Icosl-KO mice back-crossed to BALB/c mice as previously described (30) were a gift from Alison Finnegan (Rush University Medical Center, Chicago, Illinois, USA). BALB/c mice were obtained from the Jackson Laboratory. All groups of mice were age- and sex-matched. The number of animals used in each experiment is described in the figure legends.

Reagents. Recombinant proteins used in this study were as follows: human integrin αvβ3 (R&D Systems, 3050-AV), human integrin α3β1 (R&D Systems, 2840-A3), human integrin αIIbβ3 (R&D Systems, 7148-A2), human integrin αvβ5 (R&D Systems, 2528-AV), human fibronectin (R&D Systems, 4305-FNB-200), human ICOSL-His Tag (Thermo Fisher Scientific, 11559H08H50), mouse integrin αvβ3 (R&D Systems, 7889-AV-050), mouse ICOSL (Sino Biological, 50-190-M08H25),

human B7.1 (R&D Systems, 140-B1), and human ICOS (R&D Systems, 169-CS). Antibodies used were as follows: mouse anti-human αvβ3 integrin (LM609 clone; Millipore, MAB1976), rabbit anti-His tag (Rockland, 600-401-382), rabbit IgG (Gene Tex, GTX35035), mouse anti-human synaptopodin (D-9; Santa Cruz Biotechnology, sc-515842), rabbit anti-ICOSL (MyBioSource, MBS6004943), and custom polyclonal rabbit anti-ICOSL (GenScript; www.genscript.com; a peptide corresponding to amino acids YPRPNVYWINKTDNC was conjugated to KLH via an N-terminal cysteine residue and the final serum titer was >1:100,000 by ELISA). Other reagents used in this study were as follows: peptide-N-glycosidase F (PNGaseF; New England Biolabs, P0704S), cyclo [Arg-Gly_Asp-D-Phe-Val] (synthetic cRGD peptide cRGDfV; Biomol, BML-AM100), lipopolysaccharide (LPS) from *E. coli* O111:B4 (LPS-EB; Invitrogen, tlrl-eblps), streptozotocin (STZ; Sigma-Aldrich, S0130), vitronectin (Molecular Innovations, MVN-417), n-Octyl-β-D-glucopyranoside (Abcam, ab142071), and collagen I from rat tail (Gibco, A10483).

Cell culture. Immortalized human podocytes were cultured at 37°C for 10–14 days for differentiation as previously described (9). The cells were cultured in RPMI-1640 medium (Gibco, 11875) enriched with 10% fetal bovine serum (FBS; Denville Scientific, FB5001-H), insulin-transferrin-selenium (10.0 μg/ml, 5.5 μg/ml, and 6.7 ng/ml, respectively) supplement (Gibco, 41400045), 100 U/ml penicillin, and 100 μg/ml streptomycin (Gibco, A15140). Immortalized mouse podocytes were cultured according to published protocols (31). Briefly, cells were incubated in tissue culture medium (RPMI-1640 medium with 10% FBS, 100 U/ml penicillin, and 100 μg/ml streptomycin) supplemented with mouse recombinant interferon-γ (Cell Sciences, CR2041), at a concentration of 50 U/ml for the first 2 passages and then 20 U/ml for later passages, in tissue culture flasks coated with collagen I (BD Biosciences, 354236) at 33°C for proliferation. For differentiation, cells were thermoshifted to 37°C and incubated without interferon-γ for 10–14 days. For assays in the 96-well plates, human or mouse cells were differentiated at 37°C in large tissue culture flasks for 7 days prior to seeding in the appropriate well plates (i.e., 386-well plate for high-content screening assays, Figure 3A), and subsequently reseeded and incubated in multiwell plates for another 3–4 days. The cells were routinely tested for the presence of mycoplasma, and were allowed to differentiate for 10 days prior to experiments. Immortalized mouse kidney proximal tubule epithelial (TKPTS) cells (32) were obtained from Judit Megyesi (University of Arkansas for Medical Sciences, Little Rock, Arkansas, USA) and cultured in DMEM/Ham's F12 medium (Corning, 15-090-CM) supplemented with 7% FBS, 50 μU/ml insulin (Sigma-Aldrich, I5500), 100 U/ml penicillin, and 100 μg/ml streptomycin at 37°C.

Reverse transcription and quantitative polymerase chain reaction (qPCR) assays. Total RNA was isolated from cells (primary mouse podocytes, cultured mouse and human podocytes) using Trizol reagent (Invitrogen) according to the manufacturer's protocol. cDNAs were synthesized using a High Capacity cDNA Reverse Transcription Kit (Applied Biosystems, 4368813). PCR reactions were performed in triplicate using a CFX96 Real-Time System (Bio-Rad). For analysis, results were expressed as fold changes by LPS/TNF-α treatment using the gene expression levels normalized to those of *GAPDH* ($2^{-\Delta\Delta Ct}$ method). The following TaqMan gene probes purchased from Thermo Fisher Scientific were used: mouse *Icosl* (Mm00497238_m1), human *ICOSLG* (Hs00323621_m1), mouse *Gapdh* (Mn99999915_g1), and human *GAPDH* (Hs02758991_g1).

Isolation of primary podocytes. Primary mouse podocytes were isolated using Dynabeads magnetic separation as previously described

with some modifications (33). Briefly, mice were anesthetized and perfused through the heart with 20 ml Hank's Balanced Salt Solution (HBSS), which contained 8×10^7 M-450 Dynabeads (Invitrogen, 14013). Kidneys were harvested, minced into small pieces, and digested in HBSS buffer containing 1 mg/ml collagenase A (Sigma-Aldrich, C-6885) and 100 U/ml DNase I (New England Biolabs, M0303L) at 37°C for 30 minutes. Digested tissue was pressed twice though a 100-μm cell strainer (BD Biosciences, 352360), washed with HBSS buffer, then subjected to magnetic particle isolation. Isolated glomeruli were then ready to be cultured on precoated collagen I dishes for 5 days. Cells were trypsinized and filtered using a 40-μm cell strainer (BD Biosciences, 352340). Filtered cells were spun down and seeded on collagen I–coated dishes for culturing.

Production and transduction of lentivirus. Lenti ORF clone of human *ICOSL* (RC208975L2) and *ICOSL*-human shRNA constructs in lentiviral GFP vector (TL303997) targeting human *ICOSL* mRNA were obtained from OriGene. An empty lentiviral vector and scrambled negative shRNA construct were used as controls. The lentiviral constructs, along with psPAX2 (packaging) and pCMV-VSVG (envelope) vectors, were transfected into HEK-293T cells using Fugene 6 reagent (Promega) according to manufacturer's instructions. A lentivirus harboring *ICOSL* was collected from the culture media after 3 days, titrated, aliquoted, and then stored at –80°C. Nucleospin RNA virus columns (Macherey-Nagel, 740956) were used for virus RNA isolation and titration was achieved using the Lenti-X qRT-PCR Titration Kit (Clontech, 631235). For transduction of lentivirus, human podocytes were counted (5×10^5 cells) and plated onto T75 flasks. Twenty-four hours later, growth medium was aspirated and replaced with DMEM media containing lentivirus and incubated overnight. The next day, cells were replaced with complete growth media. Cells were maintained in complete growth media until cell assays were performed 30–48 hours later. Using a triplicate set, the cells were assayed for expression knock down using qRT-PCR (Supplemental Figure 7A).

Homology modeling of human and mouse ICOSL. The 3D models of ICOSL isoform 1 (extracellular domain) were constructed using a homology modeling method (SWISS-MODEL online server) with chain A of 4I0K (PDB Code, Crystal structure of murine B7-H3, PDL-1 extracellular domain) as a template, which shows the highest sequence identity as 32.2%. Restrained minimization was performed for both structures to optimize the constructed models using the Schrödinger modeling package (minimized on hydrogens first, and then RMSD of heavy atoms converged to less than 0.30 Å in OPLS3 force field).

Adhesion assays and analysis of image quantification. Bovine serum albumin (BSA, 20 μg/ml) or human ICOSL (20 μg/ml) was used to coat 348-well plates. Human podocytes were collected from tissue culture flasks and treated with β3 integrin antibody (10 μg/ml), isotype control mouse IgG (10 μg/ml), or cRGD peptide (10 μg/ml) for 15 minutes at 37°C followed by treatments with $MnCl_2$ (0.25 mM) or the appropriate combination as indicated in Figure 3A before loading into the precoated 348-well plates (human podocytes: 4000 cells/well; mouse podocytes: 5000 cells/well). After incubating for 30 minutes at 37°C, cells were then washed and fixed using a solution of 4% paraformaldehyde (PFA) in PBS for 20–30 minutes at room temperature. The cells were washed, then if needed, stained with 0.1 μg/ml (in PBS) DAPI (Invitrogen, D1306) or 2 μg/ml (in PBS) CellMask Blue (Invitrogen, H32720) to visualize nuclei and the individual cell boundaries, respectively. For each condition, assays were performed in triplicate for assay robustness. For image anal-

ysis, the podocytes were imaged using an Opera high-content image system and quantification was performed using Columbus software (Perkin Elmer) (34). To count adhered podocytes, nuclei were detected using DAPI signal, and the nuclei number was counted. The nuclei number in each well was considered the number of cells adhered.

Mouse and human ICOSL DNA constructs. The mouse full-length *Icosl* coding sequence (NM_015790, transmembrane protein) was prepared by codon-optimized synthesis for *Escherichia coli* expression (Biobasic). Briefly, the synthesized coding sequence was cloned between the NdeI and XhoI sites of the pET15b expression vector carrying an N-terminal His-Tag sequence (Novagen), verified by sequencing. Primers used for amplifying the human *ICOSL* coding sequence by PCR were as follows: (NdeI, forward: 5′-ATGCATCATATGCGGCTGGGCAGTCCT-GGACT-3′ and XhoI, reverse: 5′- ATGGATCTCGAGTTAAACGTGGC-CAGTGAGCTCTG-3′). These primers covered whole-protein sequences based on the GenBank sequence NM_015259 and were amplified from a purchased cDNA clone (OriGene, RC208975L2). The purified PCR product was subcloned into pET15b with the indicated enzyme sites and verified by sequencing. Transformation of verified plasmids into BL21 (DE3) cells (Novagen) was performed for protein purification. For mutagenesis on mouse *Icosl,* mutations were introduced by PCR using the QuickChange Lightning Site-Directed Mutagenesis kit (Agilent Technologies, 210518). The mutagenic oligonucleotides used for AAA mutation from RGD sequence, verified by sequencing, were as follows: forward: 5′-TGCGTCTGCCGTGGACCTCT-GCTGCGGCTGTTCTGTGCT-GCGTTG-3′, reverse: 5′-CAACGCAGCACAGAACAGCC-GCAGCA-GAGGTCCACGGCAGACGCA-3′.

Purification of mouse and human ICOSL protein. Protein purification was done as previously described (9), with some modifications. Briefly, each mouse and human ICOSL construct was transformed into *Escherichia coli* Rosetta2 (DE3) cells (Novagen). The cells were then induced from an exponentially growing culture by 0.5 mM isopropyl β-D-1-thio-galactopyranoside (IPTG) for 12 hours at 27°C. Cells were harvested and lysed by sonication at 65% amplitude by 100 three-second bursts separated by 6 seconds of off time (Sonic Dismembrator Model 500, Thermo Fisher Scientific) in lysis buffer (B-PER Bacterial Protein Extraction Reagent, Thermo Fisher Scientific, 90084) including 1 mg/ml lysozyme (Thermo Fisher Scientific, 89833), 0.025 mg/ml DNase I (Roche, 11284932001), and protease inhibitor cocktail (Roche, 04693124001). The His-tag fused ICOSL protein was purified using HisTrap HP column (GE Healthcare, 175247) chromatography where Ni-binding buffer (50 mM NaH_2PO_4, 500 mM NaCl, 10 mM imidazole, and 5 mM β-mercaptoethanol, pH 8.0) was applied to wash unbound impurities, followed by elution with a stepwise gradient using Ni-elution buffer (50 mM NaH_2PO_4, 500 mM NaCl, 500 mM imidazole, and 5 mM β-mercaptoethanol, pH 8.0). Fractions containing ICOSL were pooled and sequentially loaded into HiTrap QXL anion exchange columns (GE Healthcare). The ICOSL protein was eluted with a stepwise gradient using affinity buffer (50 mM Tris, 40 mM NaCl, 5 mM β-mercaptoethanol, and 0.1% n-Octyl-β-D-glucopyranoside, pH 8.0) and elution buffer (50 mM Tris, 1 M NaCl, 5 mM β-mercaptoethanol, and 0.1% n-Octyl-β-D-glucopyranoside, pH 8.0). Pure ICOSL fractions were combined, concentrated using an Amicon-Ultra-15 column (10,000 NMWL; Millipore), and buffer exchanged into PBS using a Zebra Spin desalting column (Thermo Fisher Scientific, 89889). Purity and concentration were estimated by SDS-PAGE, GelCode blue staining, and NanoDrop spectrophotometer (Thermo Fisher Scientific). Finally, the purified ICOSL protein was ali-

quoted and flash frozen as protein beads (20 μl each) in liquid nitrogen, then collected into cryovials under liquid nitrogen and stored at –80°C.

Surface plasmon resonance. Protein interactions were measured and analyzed on a Biacore T200 instrument (GE Healthcare) performed at 25°C as previously described (9). Briefly, to measure the candidate analyte proteins (integrins αvβ3, α3β1, αvβ5, or αIIbβ3) with binding affinities to mouse/human ICOSL protein (isoform 1), the full-length mouse or human ICOSL was immobilized to flow channels 2 and 3 on a CM5 sensor chip using a standard amine-coupling method. Human B7.1 and fibronectin were also used as controls. The ICOSL protein was diluted in 10 mM sodium acetate, pH 4.0, and immobilized after sensor surface activation with 1-Ethyl-3-(3-dimethylaminopropyl) carbodiimide/ N-hydroxysuccinimide) (EDC/NHS) with a 7-minute injection followed by ethanolamine blocking on unoccupied surface area. Integrin αvβ3 protein with a series of increasing concentrations (i.e., 0–160 nM at 2-fold dilution) as an analyte was applied to channels at a 20–25 μl/min flow rate at 25°C. The binding experiments were run with HEPES binding buffer (10 mM HEPES, 150 mM NaCl, 0.05% n-Octyl-β-D-glucopyranoside, pH 7.1). For the study of active status of integrin, 2 mM $MnCl_2$ or 0.2 mM $CaCl_2$ and 0.1 mM $MgCl_2$ were added to the HEPES binding buffer. For the study of inactive status of integrin, 3 mM EDTA or 2 mM $CaCl_2$ and 1 mM $MgCl_2$ were added. For inhibition assay, a constant concentration of 3 or 15 μg/ml cRGDfv was preincubated with increasing concentrations of αvβ3 integrin during sample preparation on a plate, and injected following the same procedure as previously described (9). Data were double-referenced with blank (ethanolamine) resonance unit (RU) values on flow channel 1 and zero concentration analyte signal. Sensorgrams were analyzed using the Biacore T200 evaluation software 2.0.3 and RUs were measured during the equilibration phase at each concentration for steady-state affinity fittings. Kinetic fittings were done by 1-to-1 Langmuir binding model embedded within the Biacore T200 evaluation software 2.0.3.

Immunofluorescence microscopy. Prepared human cells were seeded onto glass coverslips (Marienfeld) at 22×10^3 cells/ml in 24-well plates overnight. The following day, cells or human biopsy kidney sections from patients with FSGS or DN were rinsed with ice-cold PBS and fixed with 4% PFA for 10 minutes at room temperature followed by permeabilization with 0.1% Triton X-100 for 5 minutes. After washing with PBS twice for 5 minutes each, the coverslips were incubated with blocking buffer in 5% donkey serum (Sigma-Aldrich, D9663) and 0.3 M glycine for 1 hour at room temperature. For single/dual immunofluorescence staining, cells were incubated with custom rabbit anti-ICOSL (20 μg/ml) and/or mouse anti-human synaptopodin (1:300; Santa Cruz Biotechnology, sc-515842) at 4°C overnight. The cells were washed with cold PBS and incubated with appropriate Alexa Fluor 647–labeled donkey anti-mouse IgG (1:1000; Molecular Probes, A-31571) and/or Alexa Fluor 488–labeled donkey anti-rabbit IgG (1:1000; Molecular Probes, A-21206) secondary antibodies at room temperature for 1 hour. Cells were stained with 0.1 μg/ml (in PBS) DAPI (Invitrogen, D1306). Then cells or tissue sections were examined using an LSM 700 laser scanning fluorescence confocal microscope running ZEN software (Zeiss). Micrographs of structural markers only were adjusted uniformly in Photoshop (Adobe) using the levels function. The confocal micrographs of human kidney biopsies from healthy, early-stage DN, late-stage DN, early-stage FSGS, or late-stage FSGS were analyzed for glomerular expression of ICOSL by manually selecting glomeruli, defined by synaptopodin, as the

region of interest. Mean fluorescence intensity (MFI) was measured using ImageJ software (version 1.52a; NIH). Each disease group was normalized to healthy controls and is shown as fold change. Human podocytes were individually defined by tracing cell borders, and analyzed for ICOSL expression using ImageJ software.

Western blot analysis. PNGaseF treatment for deglycosylation of human ICOSL-His Tag protein (Thermo Fisher Scientific) was carried out following manufacturer's instructions. Approximately 50–100 ng of the protein was separated on SDS-PAGE gradient gels (NuPAGE 4%–12% Bis-Tris, Invitrogen) followed by transfer to nitrocellulose membrane (LI-COR Biosciences, 926-31092). Blots were blocked by TBS Odyssey blocking buffer (LI-COR Biosciences, 927-50000) for 2 hours at room temperature. Blots were incubated with primary antibody, rabbit anti-ICOSL (MyBiosource, 1:500), or rabbit anti-His Tag (1:1000) diluted into TBST and TBS Odyssey blocking buffer (1:1) overnight at 4°C and IRDye 680RD donkey anti-rabbit IgG (H+L) (LI-COR Biosciences, 926-68073) as secondary antibody in TBST for 1 hour at room temperature. The blotted proteins were detected using an Odyssey CLx imaging system (LI-COR Biosciences).

LPS-induced proteinuric mouse model. Proteinuria was induced with a single injection of LPS as previously described (25) with some modifications. Mice were intraperitoneally injected with LPS-EB at a dose of 2.5 mg/kg body weight.

Mouse model of STZ-induced diabetic nephropathy. BALB/c mice (8- to 12-week-old males) and age- and sex-matched *Icosl*-KO mice were given two injections of STZ (100 or 125 mg/kg body weight) at 4-day intervals as previously described (35). Briefly, the mice were fasted for 4 hours before being injected intraperitoneally with STZ dissolved in citrate buffer (pH 4.5) (Sigma-Aldrich, C8532). One to two weeks after STZ injection, mice with blood glucose values greater than or equal to 200 mg/dl were defined as STZ-induced diabetic mice. Blood glucose levels were assessed weekly. For the measurement of 24-hour urinary albumin excretion (UAE), urine samples were collected using metabolic cages.

Depletion of T cells in vivo. Anti-mouse Thy1.2/CD90.2 (BioXcell, clone 30-H12, 100 μg per mouse) or control rat IgG2a antibody (BioXcell, clone 2A3) was intravenously injected into BALB/c WT and *Icosl*-KO mice (9- to 10-week-old females and males) 24 hours prior to LPS injection (2.5 mg/kg, i.p.). Twenty-four hours after LPS treatment, the blood samples were collected and labeled with fluorescently conjugated antibodies specific for mouse CD3 (Biolegend, clone 17A2, 100214). Flow cytometric analysis was carried out using a BD LSR II with FACSDiva software (BD Biosciences), and analyzed with FlowJo software V-10 (TreeStar).

Measurement of blood glucose, ACR, and BUN levels. Blood glucose was measured from blood obtained from the tail vein of mice using a Free-Style Freedom lite glucometer (Abbott Laboratories). Mouse urine samples were collected and urinary albumin and creatinine were measured by mouse albumin ELISA kit (Bethyl Laboratories, E99-134), and creatinine assay kit (Cayman Chemical, 500701), respectively, according to manufacturers' protocols. The ratio of urinary ACR was then calculated. Serum BUN was measured using a colorimetric QuantiChrom Urea assay kit (Bioassay Systems, DIUR 100) according to the manufacturer's protocol.

Generation of bone marrow (BM) chimeric mice. BM isolation was done as previously described (25). BALB/c WT and *Icosl*-KO recipients (10- to 12-week-old females) were lethally irradiated with 9.5 Gy using a Gammacell 40 exactor (Best Theratronics) and then injected with freshly isolated BM cells from BALB/c WT and *Icosl*-KO donors (8- to 10-week-old males) (Figure 5, A and B). Mice were administered

antibiotic-treated water. Six weeks after engraftment, LPS (2 mg/kg body weight, i.p.) was injected into BM chimeric mice to induce proteinuria. Twenty-four hours after LPS injection, urine samples were collected and ACR levels were measured.

Rescue experiment. BALB/c WT and *Icosl*-KO mice (8- to 10-week-old females and males) were treated with purified mouse ICOSL protein (or BSA as a protein control) by intravenous injection at a dose of 1 mg/kg at 1 and 12 hours after LPS administration (2.5 mg/kg body weight, i.p.). Urine samples were collected at 0, 12, and 24 hours after LPS treatment for ACR measurement. To test if the renoprotective effect of ICOSL is dependent on its RGD motif, 8- to 10-week-old female and male *Icosl*-KO mice were treated with either WT (RGD) or mutant (AAA) ICOSL protein (1 mg/kg body weight, i.v.) at 1 hour following LPS injection (2.5 mg/kg, i.p.). To test the renoprotective effect of ICOSL in a type I diabetic mouse model, 8- to 10-week-old male *Icosl*-KO mice were given 2 injections of STZ (100 mg/kg body weight) at 4-day intervals. Two weeks after the first STZ injection, the mice were divided into 2 groups for the interventional study. Each group (*n* = 6/group) was treated with either mouse ICOSL protein (1 mg/kg, i.p., twice/week) or BSA as a protein control for 4 weeks. For the measurement of urinary albumin excretion, urine samples were collected using metabolic cages at 6 weeks after STZ administration (ICOSL/BSA treatment for 4 weeks).

ICOSL protein labeling and pharmacokinetic (PK) analysis. Fluorescently labeled ICOSL protein was generated by using Alexa Fluor (AF) 488 Protein Labeling Kit (Thermo Fisher Scientific, A10235) following manufacturer's instructions. Briefly, the purified mouse ICOSL protein (1 mg) was diluted in 0.5 ml of 0.1 M sodium bicarbonate buffer (pH 8.3) and transferred to a vial containing amine reactive AF488 and a magnetic stir bar. The reaction mixture was stirred for 1 hour at room temperature and then loaded onto the size-exclusion purification column prewashed with PBS. The fraction containing the labeled protein (ICOSL-AF488 conjugate) was eluted from the column and buffer exchanged into PBS using a Zebra Spin desalting column (Thermo Fisher Scientific, 89889) according to the manufacturer's protocol. To perform the plasma PK analysis for ICOSL, ICOSL-AF488 conjugate levels in the blood circulation were quantitated by measuring fluorescence in serum samples from *Icosl*-KO mice receiving a single i.v. injection. Briefly, blood samples (about 30–40 μl) were collected from the retro-orbital plexus in *Icosl*-KO mice (12-week-old females, *n* = 3) at 0.03, 0.5, 1, 3, 6, 9, and 24 hours following an i.v. administration of ICOSL-AF488 conjugate (1 mg/kg body weight). After spinning down the blood samples at 16,000 *g* for 5 minutes, sera were obtained and diluted 10-fold with PBS. A standard curve (ranging from 0.156–10 μg/ml) was prepared by using serial dilution of the injected ICOSL-AF488 conjugate with PBS containing 10% (vol/vol) control mouse serum. Fluorescence intensities of standards and diluted sera were measured at 485 nm excitation and 528 nm emission using a fluorescence plate reader (BioTek). The data at each time point were analyzed to fit to the equation for 2-phase decay using Prism version 6.0 (GraphPad).

Electron microscopy. Kidneys were dissected from LPS- and STZ-induced BALB/c WT and *Icosl*-KO mice. Renal tissue was PFA-fixed overnight at 4°C and postfixed in 1% osmium tetroxide (OsO_4) for 1 hour on ice. Tissues were washed, dehydrated, and embedded in Embed 812 Resin (EMS, 14120). Ultrathin kidney sections (70 nm) obtained on the EM UC7 Ultramicrotome (Leica) were placed on Formvar-coated Ni slot grids (EMS, FF-2010-Ni) and stained in 5% uranyl acetate and 0.1% lead citrate. EM micrographs were taken

using a Sigma HD VP Electron Microscope (Zeiss). For image analysis, foot process effacement was quantified from TEM micrographs of glomeruli as previously described (36). Briefly, multiple capillary loops were imaged at ×5000 and glomerular basement membrane (GBM) length was measured for 10 different glomeruli from a minimum of 4 mice per condition using ImageJ software (version 1.52a; NIH). To quantify effacement, secondary processes were manually tallied, and the total number of foot processes (FPs) was divided by the total GBM length to calculate FPs per micrometer of GBM.

Statistics. Statistical analysis was calculated using Prism 6.0 software (GraphPad). All *P* values less than or equal to 0.05 were considered significant (*$P < 0.05$, **$P < 0.01$, ***$P < 0.001$, ****$P < 0.0001$) and are referred to as such in the text.

Study approval. All animal experiments were carried out according to the NIH's *Guide for the Care and Use of Experimental Animals* (National Academies Press, 2011), and approved by the Institutional Animal Care and Use Committee (IACUC) at Rush University (Chicago, Illinois, USA). Human biopsy kidney sections from patients with FSGS or DN were purchased in accordance with guidelines on human research and with approval of the Institutional Review Board of Rush University Medical Center (Chicago, Illinois, USA).

Data availability. The authors declare that the data supporting the findings of this study are available within the paper and its extended data files.

Author contributions
KHK designed and performed experiments, analyzed data, and wrote the manuscript. YC performed experiments and analyzed data. SM designed experiments and contributed to writing the manuscript. NJT generated electron micrographs and analyzed data. RRD, HWL, BS, MMA, VPS, and KM contributed reagents and/or aided in performing experiments. VP contributed patient tissue samples. DJC contributed patient tissue samples and performed histological analysis. HL contributed to 3D structure modeling analysis, writing the manuscript, and SPR data analysis. JR participated in study design related to ICOSL's clinical application in kidney disease and collaborated in writing of the manuscript. EH designed and wrote the manuscript and supervised the project.

Address correspondence to: Eunsil Hahm, Department of Internal Medicine, Rush University Medical Center, 1735 W. Harrison Street, #726, Chicago, Illinois 60612, USA. Phone: 312.942.0357; Email: eunsil_hahm@rush.edu.

1. Takada Y, Ye X, Simon S. The integrins. *Genome Biol*. 2007;8(5):215.
2. Pozzi A, Zent R. Integrins in kidney disease. *J Am Soc Nephrol*. 2013;24(7):1034–1039.
3. Kreidberg JA, Symons JM. Integrins in kidney development, function, and disease. *Am J Physiol Renal Physiol*. 2000;279(2):F233–F242.
4. Fogo AB. Mechanisms of progression of chronic kidney disease. *Pediatr Nephrol*. 2007;22(12):2011–2022.
5. Reiser J, Altintas MM. Podocytes. *F1000Res*. 2016;5(F1000 Faculty Rev):114.
6. Wei C, et al. Circulating urokinase receptor as a cause of focal segmental glomerulosclerosis. *Nat Med*. 2011;17(8):952–960.
7. Wei C, et al. Modification of kidney barrier function by the urokinase receptor. *Nat Med*. 2008;14(1):55–63.
8. Staeck O, et al. Recurrent primary focal segmental glomerulosclerosis managed with intensified plasma exchange and concomitant monitoring of soluble urokinase-type plasminogen activator receptor-mediated podocyte β3-integrin activation. *Transplantation*. 2015;99(12):2593–2597.
9. Hayek SS, et al. A tripartite complex of suPAR, APOL1 risk variants and αvβ3 integrin on podocytes mediates chronic kidney disease. *Nat Med*. 2017;23(8):945–953.
10. Yoo TH, et al. Sphingomyelinase-like phosphodiesterase 3b expression levels determine podocyte injury phenotypes in glomerular disease. *J Am Soc Nephrol*. 2015;26(1):133–147.
11. Hayek SS, et al. Soluble urokinase receptor and chronic kidney disease. *N Engl J Med*. 2015;373(20):1916–1925.
12. Zhou X, et al. An integrin antagonist (MK-0429) decreases proteinuria and renal fibrosis in the ZSF1 rat diabetic nephropathy model. *Pharmacol Res Perspect*. 2017;5(5):e00354.
13. Maile LA, Gollahon K, Wai C, Dunbar P, Busby W, Clemmons D. Blocking αVβ3 integrin ligand occupancy inhibits the progression of albuminuria in diabetic rats. *J Diabetes Res*. 2014;2014:421827.
14. Maile LA, et al. Blocking ligand occupancy of the αVβ3 integrin inhibits the development of nephropathy in diabetic pigs. *Endocrinology*. 2014;155(12):4665–4675.
15. Swallow MM, Wallin JJ, Sha WC. B7h, a novel costimulatory homolog of B7.1 and B7.2, is induced by TNF-α. *Immunity*. 1999;11(4):423–432.
16. Ling V, et al. Cutting edge: identification of GL50, a novel B7-like protein that functionally binds to ICOS receptor. *J Immunol*. 2000;164(4):1653–1657.
17. Yoshinaga SK, et al. T-cell co-stimulation through B7RP-1 and ICOS. *Nature*. 1999;402(6763):827–832.
18. Wang S, et al. Costimulation of T cells by B7-H2, a B7-like molecule that binds ICOS. *Blood*. 2000;96(8):2808–2813.
19. Hutloff A, et al. ICOS is an inducible T-cell co-stimulator structurally and functionally related to CD28. *Nature*. 1999;397(6716):263–266.
20. Greenwald RJ, Freeman GJ, Sharpe AH. The B7 family revisited. *Annu Rev Immunol*. 2005;23:515–548.
21. Odobasic D, Kitching AR, Semple TJ, Holdsworth SR. Inducible co-stimulatory molecule ligand is protective during the induction and effector phases of crescentic glomerulonephritis. *J Am Soc Nephrol*. 2006;17(4):1044–1053.
22. Aicher A, et al. Characterization of human inducible costimulator ligand expression and function. *J Immunol*. 2000;164(9):4689–4696.
23. Barisoni L, Kriz W, Mundel P, D'Agati V. The dysregulated podocyte phenotype: a novel concept in the pathogenesis of collapsing idiopathic focal segmental glomerulosclerosis and HIV-associated nephropathy. *J Am Soc Nephrol*. 1999;10(1):51–61.
24. Ohtsubo K, Marth JD. Glycosylation in cellular mechanisms of health and disease. *Cell*. 2006;126(5):855–867.
25. Hahm E, et al. Bone marrow-derived immature myeloid cells are a main source of circulating suPAR contributing to proteinuric kidney disease. *Nat Med*. 2017;23(1):100–106.
26. Reiser J, et al. Induction of B7-1 in podocytes is associated with nephrotic syndrome. *J Clin Invest*. 2004;113(10):1390–1397.
27. Hall SS. Omen in the blood. *Science*. 2018;360(6386):254–258.
28. Bitzan M, Babayeva S, Vasudevan A, Goodyer

P, Torban E. TNF-α pathway blockade amelio-rates toxic effects of FSGS plasma on podocyte cytoskeleton and β3 integrin activation. *Pediatr Nephrol*. 2012;27(12):2217–2226.

29. Felding-Habermann B, Cheresh DA. Vit-ronectin and its receptors. *Curr Opin Cell Biol*. 1993;5(5):864–868.

30. Hamel KM, Cao Y, Olalekan SA, Finnegan A. B cell-specific expression of inducible costimulator ligand is necessary for the induction of arthritis in mice. *Arthritis Rheumatol*. 2014;66(1):60–67.

31. Mundel P, et al. Rearrangements of the cytoskel-eton and cell contacts induce process formation during differentiation of conditionally immor-talized mouse podocyte cell lines. *Exp Cell Res*. 1997;236(1):248–258.

32. Ernest S, Bello-Reuss E. Expression and function of P-glycoprotein in a mouse kidney cell line. *Am J Physiol*. 1995;269(2 pt 1):C323–C333.

33. Takemoto M, et al. A new method for large scale isolation of kidney glomeruli from mice. *Am J Pathol*. 2002;161(3):799–805.

34. Reiser J, Lee HW, Gupta V, Altintas MM. A high-content screening technology for quantita-tively studying podocyte dynamics. *Adv Chronic Kidney Dis*. 2017;24(3):183–188.

35. Tesch GH, Allen TJ. Rodent models of streptozo-tocin-induced diabetic nephropathy. *Nephrology (Carlton)*. 2007;12(3):261–266.

36. Lee HW, et al. Absence of miR-146a in podocytes increases risk of diabetic glomerulopathy via up-regulation of ErbB4 and Notch-1. *J Biol Chem*. 2017;292(2):732–747.